Numerical combination for nonlinear analysis of structures coupled to layered soils

Abstract

This paper presents an alternative coupling strategy between the Boundary Element Method (BEM) and the Finite Element Method (FEM) in order to create a computational code for the analysis of geometrical nonlinear 2D frames coupled to layered soils. The soil is modeled via BEM, considering multiple inclusions and internal load lines, through an alternative formulation to eliminate traction variables on subregions interfaces. A total Lagrangean formulation based on positions is adopted for the consideration of the geometric nonlinear behavior of frame structures with exact kinematics. The numerical coupling is performed by an algebraic strategy that extracts and condenses the equivalent soil's stiffness matrix and contact forces to be introduced into the frame structures hessian matrix and internal force vector, respectively. The formulation covers the analysis of shallow foundation structures and piles in any direction. Furthermore, the piles can pass through different layers. Numerical examples are shown in order to illustrate and confirm the accuracy and applicability of the proposed technique.

Keywords

BEM, FEM, soil-structure interaction, geometrical nonlinearity.

Wagner Queiroz Silva[*] **and Humberto Breves Coda**

Universidade de São Paulo, Departamento de Engenharia de Estruturas, São Carlos - São Paulo - Brazil

[*] Author email: wagner1@sc.usp.br

1 INTRODUCTION

The analysis of soil-structure interaction problems is very complex due to the large number of variables involved. To simplify a conventional building analysis, foundations are usually considered rigid supports, or approximate models, such as Winklers springs are adopted for the consideration of soil's deformability, see [9, 18]. Although this type of approximation has been commonly applied to many practical engineering problems, it does not consider the soil's continuity, and in some cases a more refined methodology is required.

Furthermore, regarding geometric nonlinear analysis of structures, it is often performed adopting approximate coefficients or simplified formulations [10]. However, for slender structures, like high-towers or high-rise buildings, simplified models may not be the most appropriate, compromising the structural analysis.

In recent years, plenty of progress has been made regarding numerical formulations applied to structural mechanics. It is important for engineers to follow this progress and to be prepared to choose appropriate structural models for modern structures design since these structures are becoming slender.

This paper presents a numerical technique for the analysis of 2D frame structures coupled to heterogeneous soils in order to create a computational program for the geometric nonlinear analysis of soil-structure interaction problems. The proposed technique may be useful for engineers as it offers a refined methodology for this type of analysis in a simple engineering language.

The soil is modeled by the Boundary Element Method (BEM) adopting an alternative sub-region technique based on [21] for the consideration of multiple inclusions and internal load lines. This strategy reduces the number of variables as it avoids contact traction approximations. The same strategy is adapted for bending plate analysis in [15, 16]. Also in [17] the alternative technique is used for tridimensional analysis of multi-region BEM elastic problems.

In the present study, internal load lines pass through different domains for the simulation of piles foundation in elastic layered soils.

The frame structure is modeled by the Finite Element Method (FEM) using the positional formulation described in [2, 6, 8]. The positional description simplicity facilitates the implementation of a Lagrangean formulation to consider the geometric nonlinear behavior of the structure with exact kinematics considering shear effects.

The numerical coupling is performed by an algebraic strategy that extracts and condenses the equivalent soil's stiffness matrix and contact forces on BEM to be respectively introduced into the frame structure's hessian and the internal force vector on FEM. Thus, the soil represents more than a simple boundary condition for the frame structure considering the cross influence of near or distant foundations.

The association of soil-structure interaction with geometric nonlinear behavior improves the structural model that can be applied to the analysis of slender structures supported on soft layered soils. Some numerical examples are shown to prove the accuracy and applicability of the proposed technique.

2   THE SOIL MODELING – BEM FORMULATION

The application of BEM to elastic problems consists basically in solving the differential equilibrium equation of an elastic solid by converting it into an integral equation on the boundary. Roughly, this procedure is performed using Gauss theorem, and results in the following boundary integral equation:

$$c_{ik}u_i\left(s\right) + \int_\Gamma p_{ik}^*\left(s,f\right)u_i\left(f\right)\,d\Gamma = \int_\Gamma p_i\left(f\right)u_{ik}^*\left(s,f\right)d\Gamma \tag{1}$$

Equation (1) is written for a source point s located inside the body domain or, occasionally over its boundary Γ and related to the field point f, where displacement u_i and traction p_i are

measured. The left term c_{ik} depends on the source point position and its determination can be performed indirectly through the rigid body concept. This equation is valid for homogeneous, isotropic and linear elastic domains and is also called Somigliana identity [1].

The integral kernels $u*_{ik}$ and $p*_{ik}$ constitute the Kelvin two-dimensional fundamental solution, representing displacements and tractions, respectively, and are given as follows:

$$u_{ik}^* = \frac{-1}{8\pi G\left(1-\nu\right)}\left\{\left(3-4\nu\right)\ln r\delta_{ik} - r_{,i}r_{,k} + \frac{\left(7-8\nu\right)}{2}\delta_{ik}\right\} \tag{2}$$

$$p_{ik}^* = \frac{-1}{4\pi\left(1-\nu\right)r}\left\{\left(1-2\nu\right)\left(n_i r_{,k} - n_k r_{,i}\right) + \left(\left(1-2\nu\right)\delta_{ik} + 2r_{,i}r_{,k}\right)\frac{dr}{dn}\right\} \tag{3}$$

where r is the distance between the source and field points, i.e. $r = |f\text{-}s|$, G is the shear elastic modulus of the material, ν is the Poisson ratio, n is the boundary normal unit vector and δ_{ik} represents the Kronecker delta.

For numerical solution, nodal approximations for u_i and p_i are taken using polynomial functions over boundary elements (appendix A), and the integral equation (1) is converted into an equivalent algebraic system as follows:

$$\mathbf{H}U = \mathbf{G}P \tag{4}$$

where matrix $\mathbf{H}$ is obtained from the left terms in equation (1) and matrix $\mathbf{G}$ from the terms on the right side. U is a vector which contains the nodal values of displacements for all boundary nodes and P is another vector for nodal values of tractions.

As there are known values of the boundary conditions (restricted displacements and applied forces) it is possible to transform equation (4) into a linear algebraic system with a possible solution, allowing the calculation of the unknown values of displacements and tractions.

Back to the fundamental solution expressions, it is important to observe that $u*_{ik}$ has a singularity order of ln*(r)*, while $p*_{ik}$ has singularity of *1/r*. It is easy to see that, the closer the source point reaches the boundary, the more equations (2) and (3) tend to infinity, leading to a mathematical singularity. In this study, the $\mathbf{H}$ matrix singularity will be solved through the rigid body concept [4]. For the $\mathbf{G}$ matrix calculation it is necessary to adopt a subtraction singularity technique as presented in [5, 11] in order to accurately perform the involved integrals over curved elements. For this technique, a fictitious element is assumed on the singular core, and a Taylor expansion allows for the division of the singular equation into two terms: a regular integral and one solved analytically.

It is also worth observing that in expression (3) the fundamental solution for traction does not depend on the G modulus, as the displacement, in expression (2) does. This information will be useful for the alternative coupling technique discussed in the next section.

As the applications of interest are soil-structure interaction problems, it is interesting to arbitrate the width of soil domain that will influence the frame structure behavior. This procedure can be performed multiplying equation (1) by the width of influence, which replaces surface forces per unit of area by surface forces per unit of length and corrects the $\mathbf{H}$ matrix to consider the width of influence.

Equation (1) is developed for homogeneous bodies. In the next section an alternative formulation for the consideration of multiple domains is presented and the implementation of internal load lines is developed.

2.1   Alternative boundary technique for sub-regions

For the elastic analysis of heterogeneous domains it is usual to adopt the widely known classical sub-region technique, which consists basically in the non-homogeneous body division according to the material characteristics of each sub-region. Each sub-region has its own system of equation (separately stored), therefore, by applying the forces equilibrium and displacement compatibility over interfaces, a unique algebraic system is written for the whole domain [3].

Although this procedure has been widely used for elastic problems with BEM, [12, 19] observed that for nonlinear problems the definition of several interfaces for a continuum domain could introduce inaccuracies in the final results due to the large number of equations. Besides, it is difficult to apply this technique to a large number of sub-regions because of the complex disposition of algebraic terms in the final system, which results in a sparse matrix.

In order to reduce the number of equations in the final system of heterogeneous bodies, [21] proposed an alternative technique that eliminates interface traction when writing the integral equation, reducing the overall number of degrees-of-freedom. From this idea, a simple algebraic strategy can be implemented in the BEM computational code for the analysis of multiple generalized inclusions.

As previously mentioned, the fundamental solution for traction, equation (3), does not depend on the G shear modulus. Considering that all involved sub-regions have the same Poisson ratio, it is possible to write a unique p^*_{ik} along all body boundaries. Besides, with an equal Poisson ratio, the u^*_{ik} solution of each sub-region j can be related to each other by dividing shear modulus j by a standard modulus, where the standard shear modulus should be the one of the predominant material. Thus, combining these ideas, it is possible to write one equation for the whole heterogeneous body, including only displacement field approximation for common interfaces.

To illustrate this procedure, consider a two sub-region domain as showed in Figure 1.
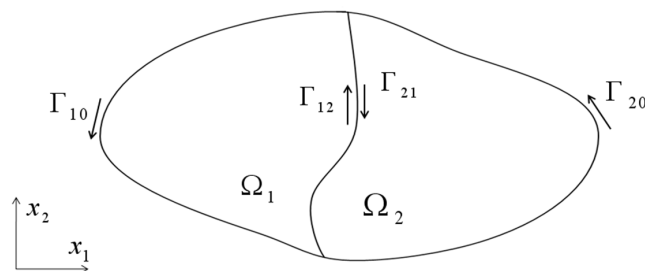

Figure 1   A two sub-region domain

The boundary of Ω_1 is divided into Γ_{10} and Γ_{12} – the latter is the contact line with sub-region Ω_2. Similarly, the boundary of Ω_2 is divided into Γ_{20} and Γ_{21}. Considering each domain

separately, but taking a unique source point, it is possible to write one integral equation for each domain, as:

$$c_{ik}^1 u_i + \int\limits_{\Gamma_{10}} p_{ik}^{*1} u_i d\Gamma_{10} + \int\limits_{\Gamma_{12}} p_{ik}^{*1} u_i d\Gamma_{12} = \int\limits_{\Gamma_{10}} u_{ik}^{*1} p_i d\Gamma_{10} + \int\limits_{\Gamma_{12}} u_{ik}^{*1} p_i d\Gamma_{12} \tag{5}$$

$$c_{ik}^2 u_i + \int\limits_{\Gamma_{20}} p_{ik}^{*2} u_i d\Gamma_{20} + \int\limits_{\Gamma_{21}} p_{ik}^{*2} u_i d\Gamma_{21} = \int\limits_{\Gamma_{20}} u_{ik}^{*2} p_i d\Gamma_{20} + \int\limits_{\Gamma_{21}} u_{ik}^{*2} p_i d\Gamma_{21} \tag{6}$$

For this hypothetical problem the sub-region Ω_1 is considered the standard domain. Although this is an arbitrary choice, it is recommended that the standard sub-region should be chosen as the predominant domain to improve the numerical accuracy.

Remembering the Kelvin fundamental solution for displacement, equation (2), and assuming the same Poisson ratio for both materials, the following relation can be written:

$$u_{ik}^{*1} = \frac{G_2}{G_1} u_{ik}^{*2} \tag{7}$$

Also, with an equal Poisson ratio, the fundamental solution for traction p^{*j} becomes unique, i.e.

$$p_{ik}^{*1} = p_{ik}^{*2} = p_{ik}^* \tag{8}$$

At this moment, both equations are multiplied by the rate between the corresponding G modulus per standard modulus, with no loss of validity. It is clear that for equation (5) there is no difference because the rate is the unity.

Thus, multiplying both sides of equation (6) by G_2/G_1 and adding equation (5), the following expression can be written for the whole body:

$$c_{ik}^1 u_i + \frac{G_2}{G_1} c_{ik}^2 u_i + \left(\int\limits_{\Gamma_{10}} p_{ik}^* u_i d\Gamma_{10} + \int\limits_{\Gamma_{20}} \frac{G_2}{G_1} p_{ik}^* u_i d\Gamma_{20} \right) + \\ + \left(\int\limits_{\Gamma_{12}} p_{ik}^* u_i d\Gamma_{12} + \int\limits_{\Gamma_{21}} \frac{G_2}{G_1} p_{ik}^* u_i d\Gamma_{21} \right) = \left(\int\limits_{\Gamma_{10}} u_{ik}^{*1} p_i d\Gamma_{10} + \int\limits_{\Gamma_{20}} \frac{G_2}{G_1} u_{ik}^{*2} p_i d\Gamma_{20} \right) + \\ + \left(\int\limits_{\Gamma_{12}} u_{ik}^{*1} p_i d\Gamma_{12} + \int\limits_{\Gamma_{21}} \frac{G_2}{G_1} u_{ik}^{*2} p_i d\Gamma_{21} \right) \tag{9}$$

On the right side of equation (9) it is possible to apply the relation given by (7) forward to the integral over Γ_{20} and backward to the integral over Γ_{12}. Then, organizing the terms, the following expression is obtained:

$$\left(c_{ik}^1 + \frac{G_2}{G_1} c_{ik}^2 \right) u_i + \int\limits_{\Gamma_{10}} p_{ik}^* u_i d\Gamma_{10} + \int\limits_{\Gamma_{12}} p_{ik}^* u_i d\Gamma_{12} + \frac{G_2}{G_1} \left(\int\limits_{\Gamma_{20}} p_{ik}^* u_i d\Gamma_{20} + \int\limits_{\Gamma_{21}} p_{ik}^* u_i d\Gamma_{21} \right) = \\ \int\limits_{\Gamma_{10}} u_{ik}^{*1} p_i d\Gamma_{10} + \int\limits_{\Gamma_{20}} u_{ik}^{*1} p_i d\Gamma_{20} + \frac{G_2}{G_1} \left(\int\limits_{\Gamma_{12}} u_{ik}^{*2} p_i d\Gamma_{12} + \int\limits_{\Gamma_{21}} u_{ik}^{*2} p_i d\Gamma_{21} \right) \tag{10}$$

Imposing the equilibrium condition on the last term of the right side of expression (10), the term in parentheses becomes null, meaning that no traction approximation is performed for the contact line reducing the number of degrees-of-freedom as desired.

The final integral equation for the heterogeneous domain without contact forces is given by:

$$
\left(c_{ik}^1 + \frac{G_2}{G_1}c_{ik}^2\right)u_i + \int_{\Gamma_{10}} p_{ik}^* u_i d\Gamma_{10} + \int_{\Gamma_{12}} p_{ik}^* u_i d\Gamma_{12} +
$$
$$
+\frac{G_2}{G_1}\left(\int_{\Gamma_{20}} p_{ik}^* u_i d\Gamma_{20} + \int_{\Gamma_{21}} p_{ik}^* u_i d\Gamma_{21}\right) = \int_{\Gamma_{10}} u_{ik}^{*1} p_i d\Gamma_{10} + \int_{\Gamma_{20}} u_{ik}^{*1} p_i d\Gamma_{20}
$$

(11)

Using a unique source point to derive equation (11) indicates that, when discretizing the whole heterogeneous domain, each source point influences all boundary elements of the problem, independently of which region it belongs to.

The illustrated example consists of only two different sub-regions, but the technique can be applied to any number of sub-regions. Indeed, by the observation of expression (11), a generalized equation can be written for ns sub-regions:

$$
\left\{\sum_{m=1}^{ns}\frac{G_m}{G_1}c_{ik}^m\right\}u_i + \sum_{m=1}^{ns}\left[\frac{G_m}{G_1}\int_{\Gamma_m} p_{ik}^* u_i d\Gamma_m\right] = \sum_{n=1}^{ne}\left[\int_{\Gamma_e} u_{ik}^{1*} p_i d\Gamma_e\right]
$$

(12)

where Γ_e is the external boundary and ne is the number of external surfaces.

For the algebraic procedure, the first thing to do is to define the predominant domain. For the chosen region, the shear modulus shall be considered G_1, and the other sub-regions may be numbered from this one.

The systems of equations for all involved sub-regions are stored using all source points of the original problem, even if the source point is not over the sub-region that is being integrated. Therefore, each sub-region system will have more rows than columns and each matrix is multiplied by the shear modulus rate. Finally, superposition is assumed, adding each sub-regions matrix to the system of the predominant domain. Because the terms of the **G** matrix (in each sub-region) related with contact interfaces were multiplied by the rate between different modulus, these terms become equal to the corresponding terms in the standard equation system. After applying the equilibrium condition of contact traction, the sum of those terms becomes null, algebraically eliminating all contact tractions. The technique is applicable to both layered sub-regions and internal inclusions.

The singularity of the **H** matrix can still be calculated using the rigid body concept, by the sum of odd and even terms of each row for each sub-region separately. For the **G** matrix, singularity is solved by a subtraction technique, as already mentioned in the previous section.

For internal points, as the original system is multiplied by the shear modulus rate, it is necessary to correct the displacement multiplying it by the inverse rate at the end of the numerical solution.

It is also possible to calculate stresses at internal points, using the Hooke constitutive law over equation (12). The following expression is obtained for stress determination on internal

collocation points:

$$\sigma_{ik}^{j} = -\sum_{m=1}^{ns} \frac{G_m}{G_j} \int_{\Gamma_j} S_{ikj}^{\star m} u_i^m d\Gamma + \int_{\Gamma_e} D_{ikj}^{*} p_i d\Gamma_e \tag{13}$$

where S_{ikj}* and D_{ikj}* are well-known tensors for the stress equation [3].

2.2 Internal Load Lines

Some engineering problems require modeling load lines inside bodies. That is the case of piles analysis in foundation engineering problems, in which the piles inserted in the soil can be modeled via FEM and act as internal load lines on BEM meshes [20].

For this type of analysis, there must be load line elements implemented in BEM formulation. However, load lines do not form closed regions and must be completely inside the body domain.

Double nodes are used in the points where load lines meet the boundary elements, avoiding the continuity of distributed forces values with different meanings (shear and normal) over each element.

Regarding tractions, load lines work exactly as boundary elements, i.e., source points integrate tractions weighted by fundamental displacements generating new columns in **G** matrix. However, as displacements are not approximated over load lines, no new column is generated in **H** matrix. Displacements at internal points are usually calculated as post processing, because the solution of the problem is only dependent on boundary values. However, when piles are connected to solids, the contact forces (tractions at load lines) are functions of pile displacements; therefore the displacements of load line nodes are directly written in the system of equations introducing source points geometrically coincident with those nodes. This procedure results in additional lines in matrix **H** including non-zero values related to boundary displacements and diagonal unit values related to domain displacements. For **G** matrix non-zero values appear for boundary and load lines columns, see equation (14). The weak singularities present in **G** matrix calculations are treated following the same procedure used for boundary elements. The final algebraic system is written as:

$$\begin{bmatrix} H_{ee} & 0 \\ H_{ie} & I \end{bmatrix} \cdot \left\{ \begin{array}{c} U_e \\ U_i \end{array} \right\} = \begin{bmatrix} G_{ee} & G_{ei} \\ G_{ie} & G_{ii} \end{bmatrix} \cdot \left\{ \begin{array}{c} P_e \\ P_i \end{array} \right\} \tag{14}$$

where index e identifies boundary terms, index i indicates internal nodes of load lines and I is the identity matrix.

The same shape functions can be adopted for the load line description as boundary elements, using Lagrange polynomials, see appendix A. These polynomials allow the use of curved internal load lines of any load order. Another advantage of load lines is that they may have any direction, making it possible to analyze inclined piles.

As for heterogeneous domains the integration procedure is affected only by the fundamental values, and the consideration of load lines trespassing regions is straightforward. First, one must identify the sub-region each load line is inserted in. Then, during the matrices storage for each sub-region, the load lines are integrated as boundary elements storing only **G** terms.

One considers a load line trespassing two regions by dividing it into two elements, each one inserted in a different domain. Superposition is still valid, and the final system includes all load lines.

3 FEM PROCEDURE

The frame structure is modeled adopting the Finite Element Method. Using the positional formulation and an intermediate non-dimensional space it is possible to apply a simple Lagrangean formulation for the consideration of geometric nonlinearity with exact kinematics. The same formulation is used in [13] for the analysis of 2D frames, assuming a nonlinear and objective engineering strain measurement for the kinematics assumption. The authors also present a comparison between Reissner and Euler-Bernoulli kinematics, checking the influence of shear deformation on bending problems.

The accuracy of positional FEM formulation has also been proved by [7, 8, 14].

In the present study, the Green strain tensor and second Piola-Kirchhoff stress are adopted. Both of them, as well as the energy functional are written as functions of the structures position. To find the equilibrium configuration, the minimum total potential energy principle is used regarding nodal position parameters.

As one can see, the FEM formulation adopted here consists basically in assuming the position of the structure as the main variable of the problem, instead of displacements. In this study, node and angular positions are assumed as the variables for each node in the finite element mesh.

3.1 Kinematics

Figure 2 presents the mapping from a non dimensional space to the initial configuration of a generic bar. This mapping is performed by Lagrange shape functions of any order (see appendix) and nodal initial positions or coordinates. The nodal initial angle indicates an orthogonal direction with respect to the mid line of the element. Function $\vec{f}_0(\xi, \eta)$ is a mapping that locates any point inside the initial domain from a point in the non-dimensional domain.

Figure 3 is a similar drawing of a generic current position of the bar. In this case the angular positions do not indicate an orthogonal direction to the reference line, but a direction that composes both bending and shear contributions to the cross-section position. In the same way, function $\vec{f}_1(\xi, \eta)$ is the mapping from the non-dimensional space to the current position.

Putting both mappings together, Figure 4 presents the desired mapping, i.e., from the initial to the current configuration.

The initial and current mappings are written for each coordinate as:

$$f_{01} = x_1(\xi, \eta) = \phi_\ell X_{1\ell} + \frac{h_0}{2} \eta \cos(\phi_k(\xi)\theta_k^0) \tag{15}$$

$$f_{02} = x_2(\xi, \eta) = \phi_\ell X_{2\ell} + \frac{h_0}{2} \eta \, sen(\phi_k(\xi)\theta_k^0) \tag{16}$$
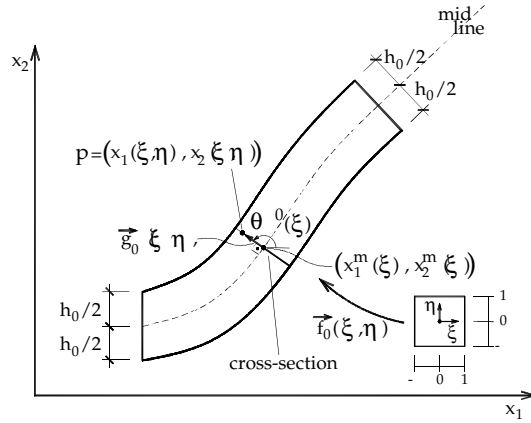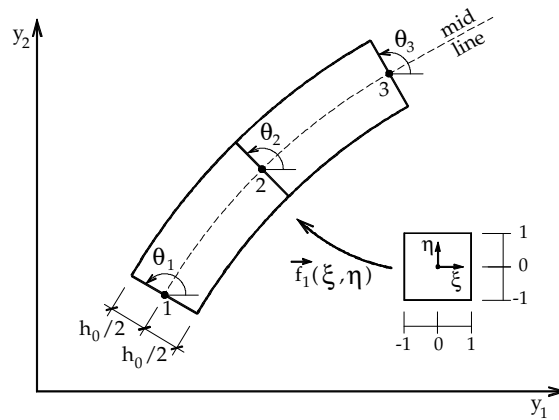
Figure 2   Initial mapping

Figure 3   Generic current position

$$f_{11} = y_1(\xi, \eta) = \phi_\ell Y_{1\ell} + \frac{h_0}{2} \eta \cos(\phi_k(\xi) Y_{3k}) \tag{17}$$

$$f_{12} = y_2(\xi, \eta) = \phi_\ell Y_{2\ell} + \frac{h_0}{2} \eta sen(\phi_k(\xi) Y_{3k}) \tag{18}$$

where x and y stand for initial and current positions, respectively, ℓ represents node and the corresponding shape function ϕ_ℓ, $X_{i\ell}$ and $Y_{i\ell}$ are the initial and current nodal positions, respectively, and θ_ℓ^0 and $Y_{3\ell} = \theta_\ell$ are initial and current nodal angular positions. Defining the current angular position as $Y_{3\ell} = \theta_\ell$ is useful to generalize the FEM solution procedure in the next section.

One may write the total mapping or the change of configuration function as:

$$\vec{f} = \vec{f}_1 \circ (\vec{f}_0)^{-1} \tag{19}$$

However, only its gradient is necessary to develop the proposed formulation, i.e.:

$$A = A^1 . (A^0)^{-1} \tag{20}$$
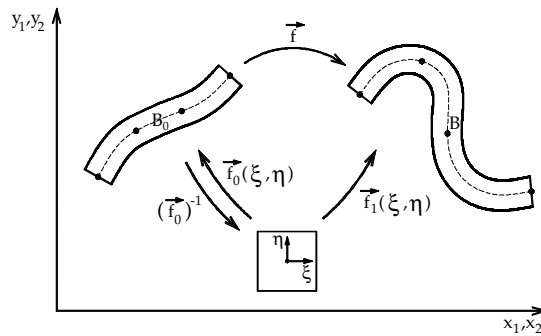
Figure 4   Positional mapping from initial to current position

where the dot indicates a simple contraction, A^1 is the gradient of the current mapping $\vec{f}_1(\xi, \eta)$ and A^0 is the gradient of the initial mapping $\vec{f}_0(\xi, \eta)$. These gradients are written as:

$$A^0 = \begin{bmatrix} \frac{\partial f_1^0}{\partial \xi} & \frac{\partial f_1^0}{\partial \eta} \\ \frac{\partial f_2^0}{\partial \xi} & \frac{\partial f_2^0}{\partial \eta} \end{bmatrix} = \begin{bmatrix} \frac{\partial x_1}{\partial \xi} & \frac{\partial x_1}{\partial \eta} \\ \frac{\partial x_2}{\partial \xi} & \frac{\partial x_2}{\partial \eta} \end{bmatrix} \tag{21}$$

$$A^1 = \begin{bmatrix} \frac{\partial f_1^1}{\partial \xi} & \frac{\partial f_1^1}{\partial \eta} \\ \frac{\partial f_2^1}{\partial \xi} & \frac{\partial f_2^1}{\partial \eta} \end{bmatrix} = \begin{bmatrix} \frac{\partial y_1}{\partial \xi} & \frac{\partial y_1}{\partial \eta} \\ \frac{\partial y_2}{\partial \xi} & \frac{\partial y_2}{\partial \eta} \end{bmatrix} \tag{22}$$

In order to achieve the Green strain tensor one calculates the right Cauchy-Green stretch tensor $\mathbf{C}$ of the change of configuration function as:

$$C = A^t.A = \left(A^0\right)^{-t}.A^{1t}.A^1.\left(A^0\right)^{-1} \tag{23}$$

and the Green strain, assumed in this study as the strain measurement, is given by:

$$E = \frac{1}{2}\left(C - I\right) \tag{24}$$

3.2   Potential energy minimization - equilibrium

As previously mentioned, the total mechanical energy should be minimized in order to solve the problem. The simple specific strain energy assumed is the so-called Saint-Venant-Kirchhoff, written in a simplified form for the analyzed problem as:

$$u_e = \frac{E}{2}\left\{\left(E_{11}^2 + E_{22}^2\right) + \left(E_{12}^2 + E_{21}^2\right)\right\} \tag{25}$$

where E is the Young modulus and E_{ij} the components of the Green strain tensor.

Therefore, the total potential energy for a conservative elastic structure is given by:

$$\Pi = U_e + P \tag{26}$$

where U_e is the elastic strain energy and P the potential energy of applied forces.

A Lagrangian description is assumed by writing the strain energy over the initial volume as follows:

$$U_e = \int_{V_0} u_e dV_0 \tag{27}$$

The potential energy of applied forces (concentrated and conservative) is written as:

$$P = -\boldsymbol{F}.\boldsymbol{Y} \tag{28}$$

As the Green strain is a function of nodal current positions (positional parameters), the same is stated for U_e and P. Applying the minimum total potential energy principle regarding positions $\mathbf{Y}$ follows the non-linear equilibrium equation:

$$\frac{\partial \Pi}{\partial \boldsymbol{Y}} = \int_{V_0} \frac{\partial u_e}{\partial \boldsymbol{Y}} dV_0 - \boldsymbol{F} = \boldsymbol{F}_{int} - \boldsymbol{F} = \boldsymbol{g} \tag{29}$$

Note that the integral over the initial volume of $\partial u_e/\partial \boldsymbol{Y}$ (for an arbitrary position) is also understood as the internal forces $\boldsymbol{F}_{int}$. Thus, $\boldsymbol{g}$ is a vector that assumes null value when the solution is obtained, i.e., when the equilibrium position of the structure is verified. However, it is understood as the unbalanced force of the mechanical system when a trial position is assumed.

For the numerical solution the Newton-Raphson procedure is used. In order to do that, a Taylor expansion from an initial trial solution Y_{arb} of g is carried out as follows:

$$g_{(Y)} = g_{(Y_{arb})} + \nabla g_{(Y_{arb})}.\Delta Y + \Theta^2 = 0 \tag{30}$$

Neglecting higher-order terms (Θ^2) and reorganizing the other terms, equation (30) can be rewritten to provide the following expression:

$$\Delta Y = -\left(\nabla g_{(Y_{arb})}\right)^{-1} g_{(Y_{arb})} = K_T^{-1}.\left(F - F_{int(Y_{arb})}\right) \tag{31}$$

where K_T is the hessian matrix or the tangent stiffness matrix, given by the second derivative of the strain energy.

The solution is achieved by assuming an arbitrary position Y_{arb} to calculate the internal forces F_{int} and the hessian matrix K_T. For the very first iteration the initial configuration X is taken as Y_{arb}.

The correction position vector ΔY is found by equation (31) and used to "correct" the arbitrary solution as follows:

$$Y_{arb+1} = Y_{arb} + \Delta Y \tag{32}$$

This new arbitrary position is assumed as the current configuration and the iterative process is carried out until $|\Delta Y|$ becomes smaller than a tolerance value. With both FEM and BEM computational codes prepared, the numerical coupling is performed for the fulfillment of this study.

4 BEM-FEM COUPLING

The numerical coupling is performed following the idea of inserting BEM's conditions in the finite element mesh by condensing the BEM algebraic system regarding coupled nodes. To do so, it is necessary to identify the coupled elements in each BEM and FEM mesh.

For the boundary element domain the following algebraic system is written:

$$\begin{bmatrix} H_{cc} & H_{cl} \\ H_{lc} & H_{ll} \end{bmatrix} \begin{Bmatrix} U_c^B \\ U_l^B \end{Bmatrix} = \begin{bmatrix} G_{cc} & G_{cl} \\ G_{lc} & G_{ll} \end{bmatrix} \begin{Bmatrix} P_c^B \\ P_l^B \end{Bmatrix} \tag{33}$$

where c is the index to identify the coupled terms and l is used for the free terms (those not coupled to the finite element mesh). The superior index B shows that those terms are related to the BEM formulation. U is a vector containing the nodal displacements and P another vector for distributed forces.

On the other hand, the finite element structure mesh is given by the algebraic system written in a simplified form as:

$$\begin{bmatrix} K_{cc} & K_{cm} \\ K_{mc} & K_{mm} \end{bmatrix} \begin{Bmatrix} U_c^F \\ U_m^F \end{Bmatrix} = \begin{Bmatrix} F_c^F \\ F_m^F \end{Bmatrix} \tag{34}$$

Again, c is related to the coupled terms. The superior index F is related to FEM formulation, and index m is used to identify the nodes which are not coupled to the boundary mesh. Vector F represents concentrated nodal forces vector. In particular U^F is related to ΔY in the iterative procedure, as a change in position is in fact a displacement.

From (33) it is possible to write two equations. Isolating U_l and organizing the result, we obtain the following expression:

$$\bar{H}_{cc} U_c^B = \bar{G}_{cc} P_c^B + T \tag{35}$$

where:

$$\bar{H}_{cc} = \left[H_{cc} - H_{cl} H_{ll}^{-1} H_{lc} \right] \tag{36}$$

$$\bar{G}_{cc} = \left[G_{cc} - H_{cl} H_{ll}^{-1} G_{lc} \right] \tag{37}$$

$$T = \left[G_{cl} - H_{cl} H_{ll}^{-1} G_{ll} \right] P_l^B \tag{38}$$

Pre-multiplying both sides of (35) by a Q_c matrix, which is originated from shape functions integration on the finite element mesh, the result does not change. The objective of Q_c matrix is to convert distributed forces P into concentrated forces F:

$$Q_c P = F \tag{39}$$

In this way it is possible to transform the boundary distributed forces into FEM nodal forces to be applied on FEM nodes. As a result of this multiplication, expression (35) becomes:

$$\bar{K}_{cc} U_c^B = F_c^B + \bar{P}_c \tag{40}$$

where:

$$\bar{K}_{cc} = Q_c \bar{G}_{cc}^{-1} \bar{H}_{cc} \tag{41}$$

$$\bar{P}_c = Q_c \bar{G}_{cc}^{-1} T \tag{42}$$

$$F_c^B = Q_c P_c^B \tag{43}$$

From (40) it is possible to isolate the equivalent applied concentrated forces from boundary elements $F_c{}^B$.

Over the interface line the following compatibility and equilibrium conditions must be imposed:

$$U_c^B = U_c^F \tag{44}$$

$$F_c^B = -F_c^F \tag{45}$$

Back to the FEM algebraic system and applying conditions (44) and (45), a final algebraic system is obtained for the coupled structure:

$$\begin{bmatrix} (K_{cc} + \bar{K}_{cc}) & K_{cm} \\ K_{mc} & K_{mm} \end{bmatrix} \begin{Bmatrix} U_c^F \\ U_m^F \end{Bmatrix} = \begin{Bmatrix} \bar{P}_c \\ F_m^F \end{Bmatrix} \tag{46}$$

This algebraic system represents the frame structure coupled to the heterogeneous soil domain. The $\bar{K}_{cc}$ matrix is understood as an equivalent soil's stiffness matrix condensed on contact nodes. Its physical significance is that soil's conditions computed in BEM model are added to the frame structure modeled by FEM as "springs". However, these "springs" have a more refined concept as they consider the soil's continuity and every condition from the BEM model, unlike Winklers approximation.

At each iteration, it is necessary to correct the internal force vector of the frame structure by adding the reaction values from soil restriction. Vector $\bar{P}_c$ has these load conditions on interface lines and will update the F_c^F vector at each iteration of the Newton-Raphson procedure.

As the soil is assumed here linear elastic, the equivalent stiffness matrix is calculated only once at the very first iteration of the nonlinear analysis.

The solid heterogeneous model is still valid, as the alternative sub-region technique is performed before the condensation of BEM algebraic system to the BEM-FEM interface.

It is important to observe that BEM formulation does not consider rotation a degree-of-freedom. Therefore, to perform the numerical coupling, null rows and columns were inserted in the BEM matrices.

Various numerical examples were processed and compared to analytical solutions or results obtained from FEM commercial software. Some of these examples are showed in the next section.

5 EXAMPLES

5.1 Tensile bar

This is a simple example of a straight bar under a tensile force. It is presented here to prove the formulation efficiency, as the result can be compared to the analytical solution.

Half of the bar is modeled via BEM and the other half via FEM, with a coupled interface in the middle section, as shown in Figure 5. The section area is unitary as a unitary width is adopted.
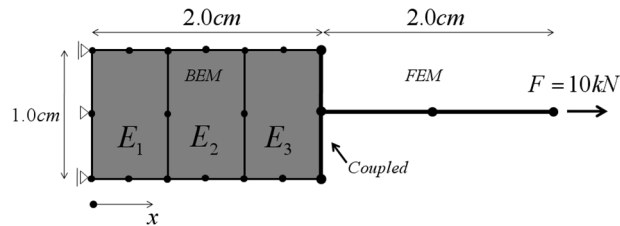

Figure 5 BEM-FEM model for straight tensile bar

The boundary mesh is divided into three domains to test the alternative technique of sub-regions. The material properties are the same for all elements, on both BEM and FEM meshes ($E_1 = E_2 = E_3 = E_{bar} = 10000 kN/cm^2$). The finite element coupled to the boundary element has thickness of 20 cm (more rigid) to allow the comparison with the analytical result. The analytical solution is given by:

$$u_{(x)} = \frac{F}{EA}x \tag{47}$$

The results are shown in Table 1.

Table 1 – Horizontal displacement (cm) along the bar length

x	BEM-FEM	Analytical	Difference %
0.00	0.00E+00	0.00E+00	-
0.33	3.334076E-04	3.333333E-04	0.02%
0.67	6.668118E-04	6.666667E-04	0.02%
1.00	1.000233E-03	1.000000E-03	0.02%
1.33	1.333483E-03	1.333333E-03	0.01%
1.67	1.664417E-03	1.666667E-03	0.13%
2.00	2.004045E-03	2.000000E-03	0.20%
3.00	3.000000E-03	3.000000E-03	0.00%
4.00	4.000000E-03	4.000000E-03	0.00%

As one can see, the connecting element flexibility allows a small difference along the central line of the BEM domain. However, results are very well compared to the references values.

5.2   Vertical pile in homogeneous domain

This is an example of a vertical pile structure inserted in a homogeneous domain and subjected to a bending moment, as it is shown in Figure 6.
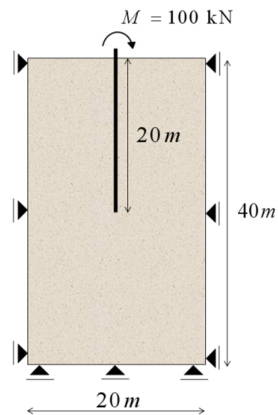

Figure 6   Vertical pile in homogeneous domain

The continuum domains Young modulus is E_s = *21000 kPa* while the pile structure's modulus is E_p = 21 *GPa*. The Poisson ratio is taken as ν = 0.2 for both soil and pile materials. A unitary influence width for the soil domain is considered and the plane stress is assumed. The pile has a circular section area with diameter D = 30 *cm*, resulting in a 706.8 cm^2 area and inertia moment of 39760 cm^4. The pile has a small length of 2.0 cm outside of soil domain on which the concentrated load is applied. A quadratic approximation is adopted for both finite and boundary elements. Two regular meshes (varying the piles discretization) are used: M1 is a mesh formed by 24 boundary elements (each element has a length of 5.0 m), and 8 finite elements (element length of 2.5 m) along the piles height; for mesh M2 50 finite elements are considered for the piles discretization (element length of 0.4 m).

The results were compared to the same example processed with the commercial ANSYS® software. For the ANSYS® model a mesh with 3200 plane stress elements was used for continuum domain's discretization and 43 conventional beam elements for the frame's mesh. The results for horizontal displacement and section rotation are presented in Figures 7 and 8.

Distributed forces along the piles length are also compared, as shown in Figure 9. The distributed force is directly obtained from the developed program. For ANSYS®, these values are obtained dividing the nodal reaction by each finite element length.

As one can see, the results compare very well despite the difference of the adopted formulations.

5.3   Pile inclined in a layered soil

An inclined pile foundation structure subjected to vertical and horizontal concentrated forces is now considered inserted in a layered soil, as shown in Figure 10.

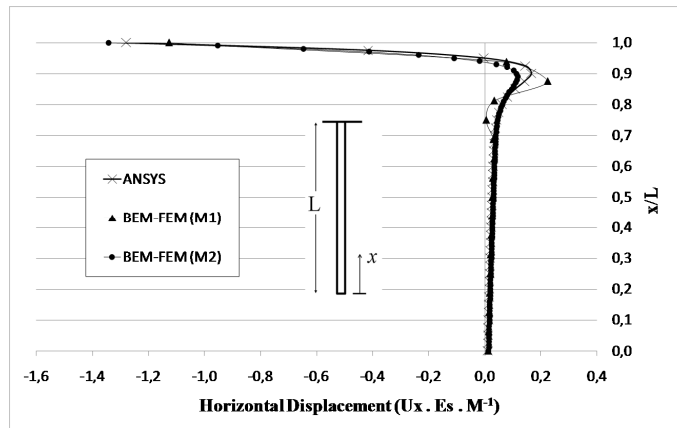The frame structure has a rectangular section of *10x15 cm* resulting in a *150 cm²* area and
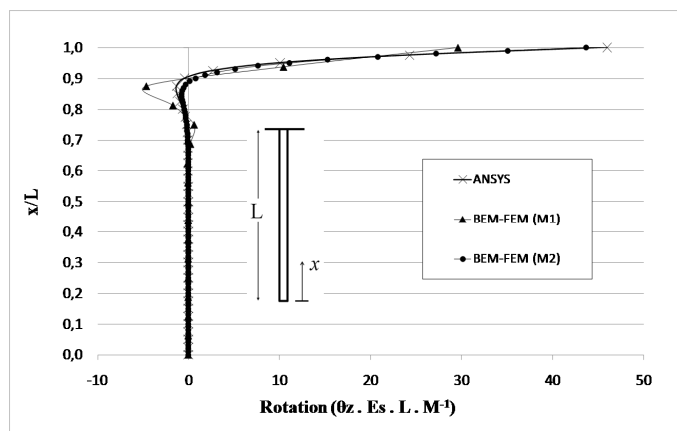
Figure 7 Horizontal displacement along the piles height

Figure 8 Rotation of sections along the piles height

inertia moment of *2812.5 cm*^{4}. The Young modulus is E_p = *2100 MPa* and Poisson ratio is null. For the soil, the elastic modulus of each layer is shown in Figure 10 and a unitary width of influence is considered.

Two regular meshes (with quadratic elements) are used: M1 is a mesh formed by 20 boundary elements and 4 finite elements along the piles height, with elements length varying from 1.0 m to 2.75 m; M2 has 210 boundary elements for the soil and 40 finite elements for the piles discretization (each element has a length of 0.1 m).

The results are again compared to ANSYS® model, with 3750 plane strain elements for the soil's mesh and 41 conventional beams elements for the pile.

For this analysis, forces F_H and F_V were separately applied and their values are F_H = *10 kN* and F_V = *-50 kN*. The pile has a small length of 2.0 cm outside of soil domain on which the concentrated load is applied.

The results for the horizontal displacement caused by F_H are shown in Figure 11. Figure
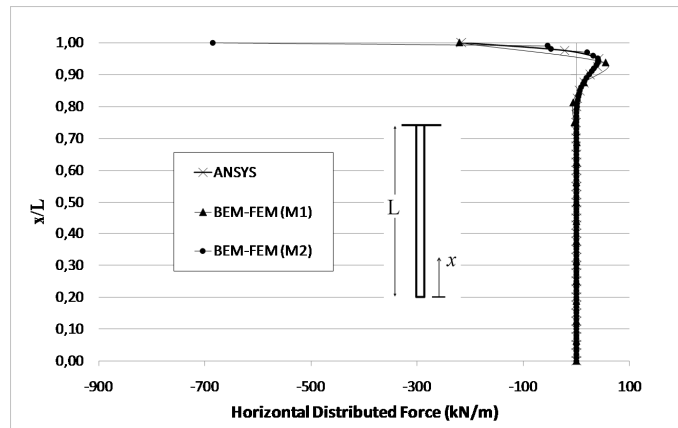
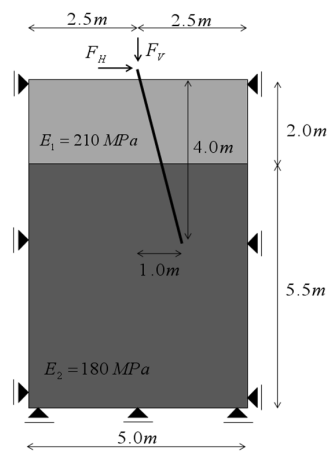Figure 9   Horizontal distributed force along the piles height

Figure 10   Pile inclined in heterogeneous soil

12 exhibits the vertical displacement caused by F_V.

There are no significant differences among the results obtained with meshes M1 and M2, which demonstrate the numerical convergence for this problem.

5.4   Bending frame

This is an example of the applicability of the proposed technique. It consists of a slender frame structure coupled to a heterogeneous soil. In this case, geometric nonlinear analysis is required to determine the structure's displacement with better accuracy. To demonstrate the importance of considering the soil-structure interaction, the results are compared to the same frame fixed by a rigid support instead of soil's domain for the contact nodes. Geometrical linear and nonlinear analyses are performed and compared.

Figure 13 presents the soil and frame dimensions and other information of interest.

The frames section is a square steel tube (*1.0 x 1.0 m*) with 3.0 cm thickness resulting in a
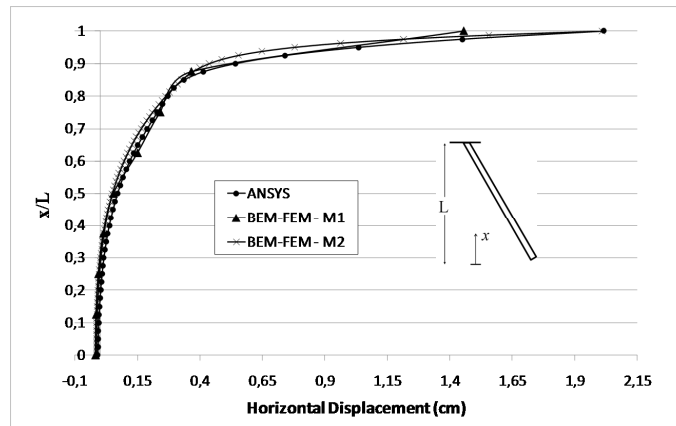
Figure 11   Horizontal displacement along the piles height caused by F_H
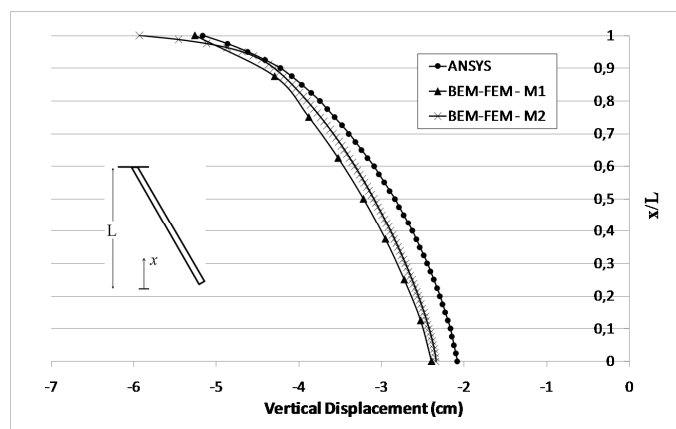
Figure 12   Vertical displacement along the piles height caused by F_V

section area of *0.1164 m²* and inertial moment of *0.0183 m⁴*. The Young modulus is $E = 210$ *GPa*. A cubic approximation is adopted for both BEM and FEM models. Two regular meshes are used, varying the discretization of the frames length inside the soil's domain: M1 is a mesh formed by 14 boundary elements and 2 finite elements along the inserted length (each finite element has a length of 7.5 m); for mesh M2 6 finite elements are considered for the inserted length, and in this case, each element has a length of 2.5 m.

The results for horizontal displacement considering linear and nonlinear analyses for the fixed support model and soil-structure interaction (SSI) model are presented in Figure 14. Note that an additional horizontal displacement is verified by considering the soil-structure interaction (SSI), as the soil's deformability influences the final results.

Table 2 shows the comparison of the maximum horizontal displacement at the top of the frame structure for linear and nonlinear analyses, for both the rigid support and soil-structure interaction (SSI) models.
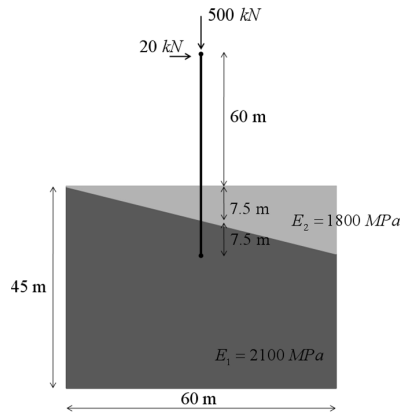
Figure 13   Slender bending frame supported by a layered soil
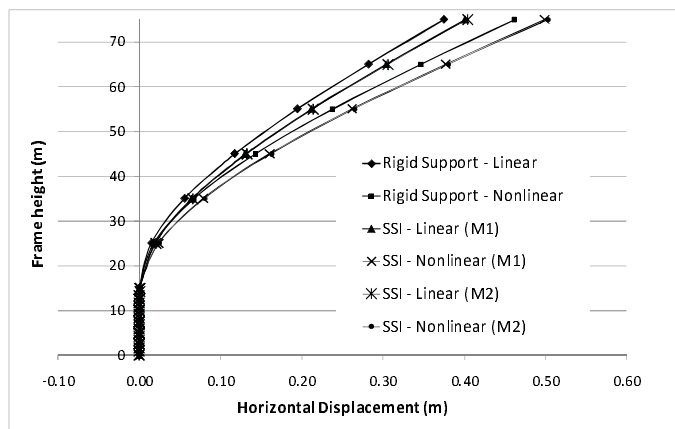

Figure 14   Horizontal displacement along the frames height

The difference between a linear analysis with rigid support and the nonlinear analysis considering soil-structure interaction is 34%, which proves that the simplified model may not be appropriate in this case.

The consideration of soil-structure interaction also leads to a different distribution the internal efforts on the frame structure model. It is interesting to measure here the influences that these differences may cause on the structural design for a safer and more economical project.

The internal normal force, shear and bending moment along the frame's height are presented next.

Also, the frames influence over the soil contact interface can be introduced into the BEM program to compute the soil final displacements and stresses. It is possible to determine the soil deformation and stress components (see Figure 18).

Table 2   Maximum horizontal displacement (cm) at the top of the structure

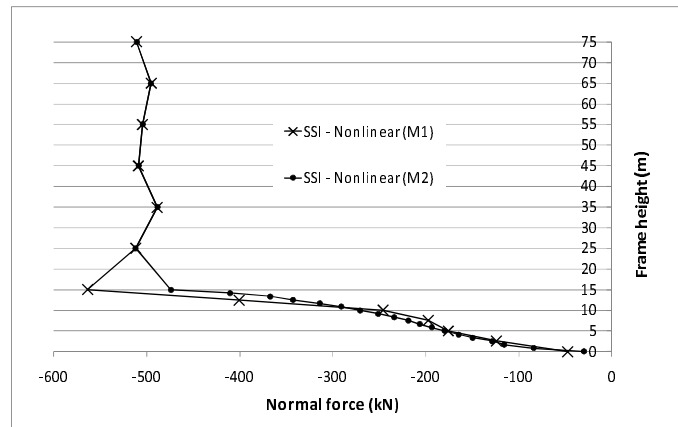| Type of analysis	Rigid Support	SSI (M1)	SSI (M2)
Linear	37.48	40.07	40.39
Nonlinear	46.14	49.88	50.31

Figure 15   Normal force along the frames height

6   CONCLUSIONS

The alternative technique for sub-regions on BEM has been successfully applied allowing for the consideration of multiple inclusions. The strategy reduces the number of variables as it eliminates the traction approximation on contact interfaces. It is possible to consider a large number of sub-regions in a much simpler way than by using the classical sub-region technique. The final matrix is compact and full. Load lines are also implemented allowing for the simulation of internal elements in any direction and passing through different domains. The FEM based on positions is used to implement a Lagrangean formulation considering the frame geometric nonlinear behavior with exact kinematics.

The developed BEM-FEM coupling introduces the linear soil influence into the frame non-linear system of equations. The main advantage of the procedure is the calculation of the matrix soil influence only once in a very compact way, reducing the amount of calculations in the iterative solution process.

The coupling strategy is more powerful than the usual Winkler procedure as it takes into account the influence of different foundations, or even buildings, on each other. Moreover the use of BEM is much more economical than the use of FEM to model the soil. Examples show the good behavior of the procedure when compared to a generalist commercial package, as ANSYS$^{\circledR}$ for instance.

Moreover, this study has emphasized the importance of the influence of the soil's flexibility on the nonlinear behavior of structures. It is important to mention the two-dimensional characteristic of the presented model, i.e., the considered soil width for all analyses is taken
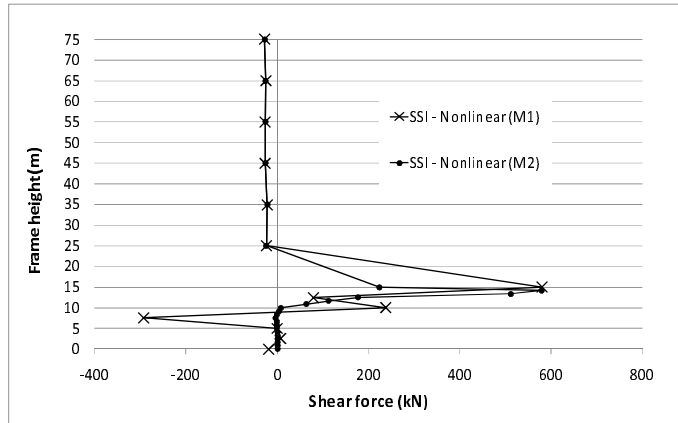
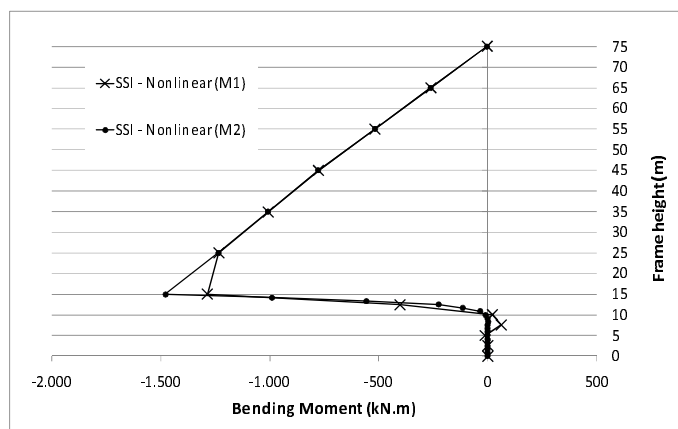Figure 16   Shear force along the frames height

Figure 17   Bending moment along the frames height

arbitrarily. In the future this formulation should be extended for 3D representation in order to provide more generality to the proposed methodology.

APPENDIX A – HIGH-ORDER ELEMENTS WITH LAGRANGE POLYNOMIALS

Both BEM and FEM formulation are implemented with high-order elements, assuming Lagrange polynomials for shape functions description. The Lagrange polynomials are given as follows:

$$\phi_l = \prod_{\substack{i \neq k \\ i = 1}}^{n} \left(\frac{\xi - \xi_i}{\xi_k - \xi_i} \right) \tag{48}$$

where ϕ_l is the l shape function for each k node of a *(n-1)* order element. The ξ coordinates
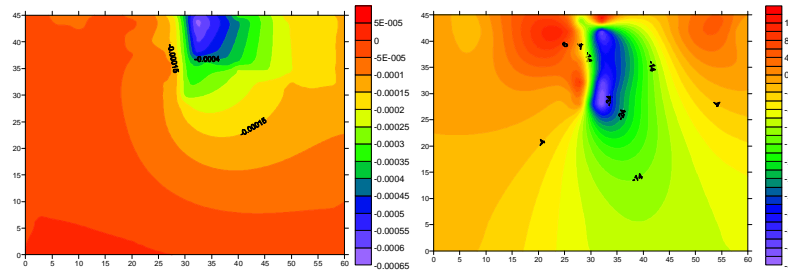
Figure 18 (a) Soil deformation in meters and (b) vertical stress component in kPa

assume values from *-1* to *+1* on dimensionless space. Therefore, it is possible to define any point of the element from its ξ coordinates.

A numerical subroutine based on equation (48) is implemented in both BEM and FEM computational codes to generate all shape functions of discrete elements. The user must only introduce the desired order for the discrete elements and the number of points for Gaussian quadrature.
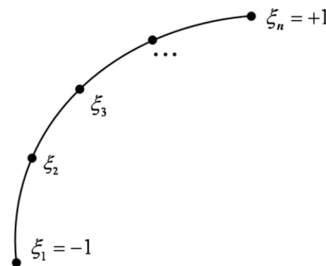

Figure 19 Curved element in dimensionless coordinates

References

[1] M.H. ALIABADI. *The boundary element method. Applications in solids and structures.* J. Wiley, Chichester, New York, 2002.

[2] J. BONET. Finite element analysis of air supported membrane structures. *Comput. Methods Appl. Mech. Eng*, 190:579–595, 2000.

[3] C.A. BREBBIA and J. DOMINGUEZ. *Boundary elements: and introductory course.* Computational Mechanics Publications, London, 1992.

[4] C.A. BREBBIA, J.C.F. TELLES, and L.C. WROBEL. *Boundary Element Techniques.* Springer Verlag, Berlin, 1984.

[5] H.B. CODA. Contribuiçãoo à análise dinâmica transiente de meios contínuos pelo método dos elementos de contorno. tese (livre docência), 2000.

[6] H.B. CODA. *An exact FEM geometric non-linear analysis of frames based on position description. In: XVIII.* Congresso Brasileiro De Engenharia Mecânica, São Paulo, 2003.

[7] H.B. CODA. Two dimensional analysis of inflatable structures by the positional fem. *Latin American Journal of Solids and Structures*, 6:187–212, 2009.

[8] H.B. CODA and M. GRECO. A simple fem formulation for large deflection 2d frame analysis based on position description. *Computer Methods in Applied Mechanics and Engineering*, 193:3541–3557, 2004.

[9] H.El. GANAINY and M.H.El. NAGGAR. Efficient 3d nonlinear winkler model for shallow foundations. *Soil Dynamics and Earthquake Engineering*, 29(8):1236–1248, 2009.

[10] H.SCHOLZ. Approximate p-delta method for sway frames with semi-rigid connections. *J. Construct. Steel Research*, 15:215–231, 1990.

[11] A. K. L. KZAM. Formulação dual em mecânica da fratura utilizando elementos de contorno curvos de ordem qualquer. dissertação (mestrado), 2009.

[12] J.C. LACHAT. Effective numerical treatment of boundary-integral equations: A formulation for three-dimensional elastostatics. *Int. J. Numer. Methods Eng*, 10:991–1005, 1976.

[13] MACIEL, Daniel Nelson, and H.B. CODA. Positional finite element methodology for geometrically nonlinear analisys of 2d frames. *Revista Minerva*, 5:73–83, 2008.

[14] R. L. MINSKI. Aprimoramento de formulação de identificação e solução do impacto bidimensional entre estrutura e anteparo rígido. dissertação (mestrado), 2008.

[15] J.B. PAIVA and M.H. ALIABADI. Boundary element analysis of zoned plates in bending. *Comput Mech*, 25:560–6, 2000.

[16] J.B. PAIVA and M.H. ALIABADI. Bending moments at interfaces of thin zoned plates with discrete thickness by the boundary element method. *Eng Anal Boundary Elem*, 28:747–51, 2004.

[17] D.B. RIBEIRO and J.B. Paiva. An alternative multi-region bem technique for three-dimensional elastic problems. *Engineering Analysis with Boundary Elements*, 33:499–507, 2009.

[18] R.A. SOUZA and J.H.C. REIS. Interação solo-estrutura para edifcios sobre fundações rasas. *Acta Sci. Technol., Maringá*, 30(2):161–171, 2008.

[19] W.S. VENTURINI. *Boundary Element Method In Geomechanics*. Springer-Verlac, Berlin, 1984.

[20] W.S. VENTURINI. Um estudo sobre o método dos elementos de contorno e suas aplicações em problemas de engenharia. tese (livre docência), 1988.

[21] W.S. VENTURINI. Alternative formulations of the boundary element method for potential and elastic problems. *Engineering Analysis with Boundary Elements*, 9:203–207, 1992.